



**HAL**  
open science

# Prebiotic membrane structures mimic the morphology of purported early traces of life on Earth

Seán F Jordan, Mark A van Zuilen, Joti Rouillard, Zita Martins, Nick Lane

## ► To cite this version:

Seán F Jordan, Mark A van Zuilen, Joti Rouillard, Zita Martins, Nick Lane. Prebiotic membrane structures mimic the morphology of purported early traces of life on Earth. 2023. hal-04308482

**HAL Id: hal-04308482**

**<https://hal.science/hal-04308482>**

Preprint submitted on 27 Nov 2023

**HAL** is a multi-disciplinary open access archive for the deposit and dissemination of scientific research documents, whether they are published or not. The documents may come from teaching and research institutions in France or abroad, or from public or private research centers.

L'archive ouverte pluridisciplinaire **HAL**, est destinée au dépôt et à la diffusion de documents scientifiques de niveau recherche, publiés ou non, émanant des établissements d'enseignement et de recherche français ou étrangers, des laboratoires publics ou privés.

# 1 **Prebiotic membrane structures mimic the morphology of purported early traces of life on Earth**

2

3 Seán F. Jordan<sup>1,2,3\*</sup>, Mark A. van Zuilen<sup>4</sup>, Joti Rouillard<sup>5</sup>, Zita Martins<sup>2</sup>, and Nick Lane<sup>3</sup>

4

5 <sup>1</sup>*Life Science Institute, School of Chemical Sciences, Dublin City University, Glasnevin, Dublin 9, Ireland*

6 <sup>2</sup>*Centro de Química Estrutural, Institute of Molecular Sciences and Department of Chemical  
7 Engineering, Instituto Superior Técnico, Universidade de Lisboa, 1049-001 Lisboa, Portugal*

8 <sup>3</sup>*Centre for Life's Origin and Evolution, Department of Genetics, Evolution and Environment, Darwin  
9 Building, Gower Street, University College London, London WC1E 6BT, UK*

10 <sup>4</sup>*CNRS-UMR6538 Laboratoire Geo-Ocean, Institut Universitaire Européen de la Mer, Université de  
11 Bretagne Occidentale, Plouzané, France*

12 <sup>5</sup>*Ecole Nationale Supérieure de Géologie de Nancy, Université de Lorraine, Vandoeuvre-lès-nancy,  
13 France*

14

15 **\*Corresponding author:** Seán F. Jordan [sean.jordan@dcu.ie](mailto:sean.jordan@dcu.ie)

16

17 **Key words:** origin of life, micropalaeontology, lipid vesicles, microfossils, biomorphs, biosignatures,  
18 prebiotic chemistry, geobiology, protocells, protobiosignatures

19

## 20 **Abstract**

21 Elucidating the most probable compositions of the first cell membranes prior to the origin of life,  
22 within a laboratory setting, requires experiments with organic molecules and chemical conditions  
23 representative of those present on the early Earth. As such, the membrane forming molecules used  
24 in these experiments are described as 'prebiotically plausible', i.e., they could have formed through  
25 abiotic reactions and be available for membrane formation prior to the emergence of biology.  
26 Similarly, the chemical properties of solutions in which these membranes are formed (e.g., pH,  
27 temperature, ionic strength) must represent the early Earth environmental conditions under  
28 investigation. Here, using a combined confocal and transmission electron microscopy approach, we  
29 show that prebiotically plausible organic molecules, in solutions representative of Hadean submarine  
30 alkaline hydrothermal vents, form aggregated structures with substantial morphological diversity. The  
31 structures hold the potential for use as traces of prebiotic processes in the ancient rock record. In  
32 addition, many of the structures are morphologically similar to those which are presented as early  
33 microfossils, thus highlighting the limitations of morphological interpretation in these types of studies.

34 Detailed analyses of abiotic organic structures are essential for our understanding of the earliest living  
35 organisms on Earth, as well as for our interpretation of any potential biosignatures recovered in the  
36 future from extra-terrestrial bodies.

37

### 38 **1. Introduction**

39 There are many theories that exist as to how life on Earth arose. Whether in hot springs on land<sup>1</sup> or  
40 hydrothermal vents on the ocean floor<sup>2,3</sup>, all these ideas require an energy source within a geological  
41 setting that can fuel chemical reactions. Over time these reactions increased in complexity from  
42 geochemistry to organic chemistry, eventually leading to biochemistry with the emergence of life. The  
43 gradients within these settings could potentially drive chemical reactions producing organic molecules  
44 from inorganic reactants (e.g.,<sup>4-7</sup>). Organic compounds then reacted together forming more complex  
45 molecules through increasingly advanced pathways, eventually becoming something like a metabolic  
46 pathway: a protometabolism<sup>8</sup>. Without boundaries, this protometabolism may not have been long  
47 lived. Products could have quickly become diluted, and reactions could have dissipated giving way to  
48 alternate reactions. Like the cell membranes found in all living organisms, some form of  
49 compartmentalisation would probably have been required. The cell membranes of all extant living  
50 organisms are composed of glycerol phosphate phospholipids<sup>9</sup>. However, these phospholipid  
51 membranes are possibly too complex to have formed at the earliest stages of the emergence of life  
52 on Earth. Instead, early compartments could have been supplied in the form of vesicles, membrane  
53 structures composed of single chain amphiphiles (SCAs) such as fatty acids<sup>10</sup>, giving rise to the first  
54 protocells.

55 It is likely that fatty acids, alcohols, and many other SCAs would have existed in almost any  
56 origin of life scenario, and the precursors of membrane-forming molecules may have been synthesised  
57 abiotically on the early Earth<sup>11</sup>. The list of prebiotically plausible organics is ever-growing due to results  
58 from both laboratory experiments and analysis of real samples<sup>12</sup>. Prebiotic synthesis experiments  
59 have achieved the formation of carboxylic acids, amino acids, sugars, and nucleotides<sup>4,5,13-23</sup>. For  
60 example, Fischer-Tropsch-Type (FTT) syntheses under hydrothermal conditions produce numerous  
61 fatty acids, alcohols, and alkanes containing 6 to 34 carbon atoms<sup>13</sup>, all of which are suitable  
62 membrane-forming components. Carboxylic acids and amino acids of abiotic origin have been  
63 detected in rock samples from Earth, while numerous organic molecules including both aliphatic and  
64 polyaromatic hydrocarbons (PAHs), hydroxy acids, nucleobases, and amino acids have been detected  
65 in meteorites<sup>24</sup>. Carbonaceous meteorites contain fatty acids, including aliphatic straight-chain and  
66 branched-chain monocarboxylic, with up to 12 carbon atoms, and dicarboxylic acids<sup>25,26</sup>. The straight-

67 chain monocarboxylic acids are dominant, followed by the branched-chain monocarboxylic acids, and  
68 finally the dicarboxylic acids. Meteoritic monocarboxylic acids are enriched in deuterium and  $^{13}\text{C}$ ,  
69 which is consistent with an extra-terrestrial origin. It has been suggested that gas phase reactions in  
70 the interstellar medium, involving radicals and ions, synthesised meteoritic monocarboxylic acids  
71 before being accreted in the parent body of meteorites for further processing<sup>27,28</sup>. Carboxylic and  
72 dicarboxylic acids can also be formed in the meteorite parent body by two ways: 1) via hydrolysis of  
73 carboxamides<sup>29</sup>; or 2) by the oxidation of hydrocarbons from the macromolecular insoluble organic  
74 matter (IOM), or the oxidation of free hydrocarbons by oxidised fluids or minerals<sup>30</sup>. Vesicles have in  
75 fact been formed directly from organics contained within meteorite samples<sup>31,32</sup>. The meteorite flux  
76 to the Earth was much higher during the Hadean than it is today and may have spiked between 4.1  
77 and 3.8 Ga<sup>33,34</sup>. The vast amount of material delivered to the early Earth during this time represents  
78 a significant source of organic molecules. Coupled to organics formed *in situ* on the early Earth, it is  
79 probable that a wide range of compounds would have been available for membrane formation.

80 Multiple different early Earth environments have been proposed as possible settings for the  
81 emergence of the first living organisms. Each of these scenarios brings with it a unique set of  
82 conditions that would potentially affect the production and survival of organic molecules, the  
83 formation of membranes and the diversity of possible prebiotic chemical reactions. Deep sea locations  
84 with hydrothermal activity could provide a supply of organics through FTT syntheses, with high  
85 temperature acidic fluids in ‘black smokers’ and lower temperature alkaline fluids in ‘white smokers’  
86 providing very different pathways for eventual chemical reactions. Some of these sites may have been  
87 too deep for meteoritic organic delivery, while being protected from their impacts. Conversely,  
88 terrestrial hot springs are exposed to impacts, while simultaneously being receptive to extra-  
89 terrestrial organic delivery. Depending on their geology, these surface sites would have unique pH,  
90 temperature, and ionic species in their fluids, each combination of which could be amenable to  
91 different modes of prebiotic chemistry. These are just two examples of myriad possibilities. It is clear  
92 that the permutations of environmental conditions for potential origin of life locations on the early  
93 Earth are vast.

94 Despite this, the majority of work on membrane formation to date has focused on the analysis  
95 of vesicles formed from single molecules or simple mixtures containing at most two to three SCAs.  
96 The resulting vesicles struggle to survive under environmental stresses such as pH, temperature, and  
97 ionic strength fluctuations<sup>35–38</sup>. Sensitivity to salinity, in particular, has cast doubt on any oceanic  
98 environment as a possible origin of life location. Recent work, however, has found that SCAs with  
99 novel headgroup moieties can withstand some more challenging conditions including high ionic  
100 strength and extremes of pH, particularly at acidic levels<sup>39</sup>. It has also been shown that combining

101 simple SCAs in relatively complex mixtures, arguably more relevant to a prebiotic scenario, produces  
102 vesicles with significant resilience to multiple environmental stresses, including salinity and high pH<sup>40</sup>.  
103 Considering the wide range of available SCAs and the vast amount of research that remains to be done  
104 on vesicle formation capabilities, it is clearly unreasonable to exclude any potential origin of life  
105 environment based on current knowledge. In fact, it now appears likely that vesicles would have  
106 formed in almost any prebiotic scenario.

107 Vesicles display a diverse range of morphologies, both on an individual level and as aggregates  
108 or clusters of multiple vesicles<sup>40,41</sup>. These morphologies seem to be affected by environmental  
109 conditions. However, this has not been systematically investigated yet. In fact, the primary objective  
110 of origin of life membrane formation studies – testing the ability of membrane formation – has meant  
111 that these structures have been overlooked, often regarded as failed experiments. Many of these  
112 assemblages are reminiscent in their morphology of living organisms and ancient microfossils. Similar  
113 forms created entirely from self-assembled nanocrystalline materials have been described  
114 previously<sup>42–45</sup>. It has been suggested that these inorganic ‘biomorphs’ may be observed within the  
115 rock record and could be misinterpreted as microfossils of ancient living organisms. The same could  
116 be true for organic assemblages of vesicles, and perhaps for biomorphs formed through combinations  
117 of both organic and inorganic compounds.

118 Here we show that combinations of prebiotically plausible organic molecules, in solutions  
119 chemically representative of a potential early Earth environment, form a variety of complex aggregate  
120 structures. Confocal and electron microscopy reveal the morphological diversity of these structures  
121 and the similarities they hold with purported microfossils of the earliest living microorganisms on  
122 Earth. We highlight the potential for these abiotic structures as diagnostic signatures in their own  
123 right, while also highlighting their tendency to mimic microfossils in the rock record. Population  
124 morphometry results from organic biomorphs and microbial populations show strong similarities in  
125 2D structure. However, differences in population size distribution suggest that this characteristic may  
126 be useful in distinguishing between abiotic and biological microstructures of this type. Caution is  
127 required when investigating signatures of this nature and significantly more work is required to  
128 understand these abiotic structures sufficiently, to ensure that they do not hinder our interpretation  
129 of biosignatures both on Earth, and potentially elsewhere in our Solar System in the future.

130  
131  
132  
133  
134

## 135 **2. Methodology**

136

### 137 **2.1 Materials**

138 All reagents used in this study were of analytical grade ( $\geq 97\%$ ) and were procured from either Sigma  
139 Aldrich (Merck, UK) or Acros Organics (UK).

140

### 141 **2.2 Preparation of vesicle solutions**

142 The vesicle solutions were prepared employing a modified version of the technique described by  
143 Monnard and Deamer (2003)<sup>46</sup>. Glass vials were employed for all solution preparations in a dry heating  
144 block maintained at a temperature of 70 °C. This temperature corresponds to the conditions expected  
145 at Hadean alkaline hydrothermal vents (50 – 100 °C)<sup>47</sup>. The molecules used were fatty acids and 1-  
146 alkanols (C<sub>10</sub> to C<sub>15</sub>, odd and even), and the isoprenoid molecules geranic acid and geraniol. The lipids  
147 were heated and introduced to the solutions in their liquid state. Acid molecules were first added to  
148 deionized (DI) H<sub>2</sub>O to provide the desired final concentration and subjected to vortexing.  
149 Subsequently, 1 M NaOH was added until the solution turned transparent, indicating complete  
150 deprotonation of the acid. The alcohols were then added, and the solution was vortexed. The pH was  
151 adjusted by employing 1 M HCl or 1 M NaOH to achieve the desired final value. The solution was then  
152 brought to the desired final volume by adding DI H<sub>2</sub>O. Immediate analysis of solutions was conducted  
153 after their preparation.

154

155 For the preparation of vesicles in salt solutions, the H<sub>2</sub>O was substituted with the desired salt  
156 concentration, and the acid and base solutions were substituted with the salt dissolved in 1 M HCl and  
157 1 M NaOH, respectively, to ensure consistent salt concentrations throughout. Anoxic vesicle solutions  
158 (H<sub>2</sub>O, FeCl<sub>2</sub>, Na<sub>2</sub>S, FeS, Fe particles) were prepared following the aforementioned method in an  
159 anaerobic hood with a 5% H<sub>2</sub> in N<sub>2</sub> atmosphere. O<sub>2</sub> was eliminated by reacting with H<sub>2</sub> to form H<sub>2</sub>O  
160 vapour on a Pd catalyst. O<sub>2</sub> levels were monitored and maintained at 0 ppm throughout these  
161 procedures. FeS solutions were prepared using a 1:1 ratio of FeCl<sub>2</sub> and Na<sub>2</sub>S. Fe particles were added  
162 to the relevant solutions after vesicle formation in H<sub>2</sub>O. All anoxic solutions were sealed with lids and  
163 wrapped in parafilm. The seal was broken immediately before imaging.

164

### 165 **2.3 Confocal microscopy**

166 Confocal microscopy was conducted using a Zeiss LSM-T-PMT 880 instrument coupled to an Airyscan  
167 detector. Membranes were visualised using the hydrophobic dye Rhodamine 6G. 0.5 µL of a 100 µM  
168 dye solution was added to a heated (70 °C) microscope slide. The vesicle solution was vortexed, and

169 a 5  $\mu$ L aliquot was added to the slide, mixed with the dye. The aliquot was covered with a #1.5, 16 mm  
170 diameter coverslip and positioned on the microscope stage. The dye was excited using an Ar laser  
171 operating at 514 nm and observed through a 63x oil objective with a 488 nm filter. Images were  
172 captured using Zeiss Zen microscopy software, and final processing was conducted using the FIJI (Fiji  
173 is just ImageJ) software package.

174

#### 175 **2.4 Negative Staining – Transmission Electron Microscopy (NS-TEM)**

176 NS-TEM was performed using a JEOL 1010 TEM (JEOL, Japan). Samples were applied to a Cu 100 mesh  
177 grid and allowed to incubate for 30 seconds. Excess sample was then removed by blotting with filter  
178 paper, and a portion of aqueous uranyl acetate (1.5%) was added to the grid. After standing for 30  
179 seconds, the excess liquid was blotted. Grids were immediately analysed under vacuum. Image  
180 processing was carried out using the FIJI software package.

181

#### 182 **2.5 Cryo-electron microscopy (Cryo-EM)**

183 Samples were prepared using a Vitrobot Mark IV (Thermo Fisher). An aliquot was applied to a glow-  
184 discharged Lacey Carbon (400 mesh Cu) grid (Agar Scientific) for 30 s, blotted for 8.5 or 11 s at 4.5  $^{\circ}$ C  
185 and 95% humidity, and then rapidly plunged into liquid ethane. Imaging was performed on a T10  
186 microscope (FEI) at 100 kV. Images were collected at a magnification range of 7000-34000x.

187

#### 188 **2.5 Population morphometry**

189 Population morphometry analysis<sup>43,48,49</sup> was performed on several images of the experiments,  
190 following the protocols described in Rouillard et al. (2020)<sup>49</sup>. All image treatment was carried out using  
191 FIJI version 1.53t. Some improvements in image segmentation were implemented, relative to  
192 Rouillard et al. (2020)<sup>49</sup>, particularly making use of machine learning trainable segmentation and  
193 threshold binarization. The individual steps of morphometric analysis are described below:

194

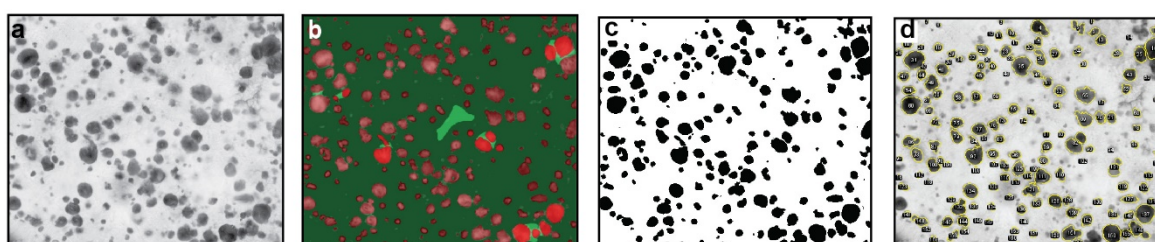
##### 195 *2.5.1 Image segmentation*

196 Using FIJI, each image was cropped to exclude scale bars and other annotated features. For some  
197 images with uneven background shading, a subtraction of background noise was performed using the  
198 Subtract Background process (using a rolling ball radius of approximately the size of the particles).  
199 Further optimisation before segmentation depended on the individual image. This included image  
200 inversion (Fig. S1b), an additional Gaussian blur to make cells stand out relative to artifacts (Fig. S2b),  
201 or edge-detection (using the Canny Edge plugin) followed by hole-filling (Fig. S3c).



202 Subsequently the Trainable Weka Segmentation plugin<sup>50</sup> was loaded. The classifier training process  
203 was initiated using two classes, one for the structures of interest and another for background (Fig. 1;  
204 Fig. S1 c, d; Fig. S2 c, d). The classifier was trained to fill holes and to separate touching cells. In some  
205 images it was more effective to classify artifacts that obscured the cells (Fig. 3; Fig. S3c-f). In that case  
206 an image was created that could be subtracted from the pre-Weka image, resulting in a cleaned-up  
207 version showing only the particles of interest. For all Weka-segmented images a binarized segmented  
208 image was then created (Fig. S1e, S2e, S3g). Individual particles could then be counted using the  
209 Analyze Particles option, selecting area and shape descriptors. The major steps of this protocol are  
210 shown in Figure 1.

211



212

213 *Figure 1. Major steps in image segmentation and particle counting protocol. Experimental vesicles*  
214 *(dried). a) Original, cropped image, b) Weka trainable segmentation, separating individual cells from*  
215 *background, c) thresholding and binarization, d) Particle counting, size and shape description. For more*  
216 *details on segmentation, see Figure S1.*

217

### 218 2.5.2 Particle characterization

219 Following Rouillard et al. (2020)<sup>48</sup>, for each segmented image the entire population of particles was  
220 counted (using a 5-pixel size threshold to avoid small dots), and for each particle the area (A) (in square  
221  $\mu\text{m}$ ), radius (R) (assuming a perfect circle, in  $\mu\text{m}$ ) circularity (C) and solidity (S) were determined.  
222 Circularity is defined as  $C = 4\pi A/P^2$ , where P (in pixels) is the circumference of the particle. Solidity is  
223 defined as  $S = A/\alpha$  where  $\alpha$  is the area (in square pixels) within the convex hull of the particle. This  
224 convex hull consists of the surface bound by straight lines that join the outermost points of the  
225 particle.

226

## 227 Results

228 A selection of prebiotically plausible and biochemically important single chain amphiphilic organic  
229 molecules were used to investigate the formation of abiotic structures (Table 1). Different  
230 combinations of organics, pH and additional ionic species were used for each solution prepared.  
231 Molecules were first dissolved in alkaline (pH ca. 11) aqueous NaOH solutions. This pH is sufficiently



232 above the pKa of the individual molecules to provide solutions so that the organics exist as monomers  
233 or micelles. The solutions were titrated with 1 M HCl to encourage bilayer formation leading to the  
234 development of individual vesicles and more complex structural assemblages. Confocal micrographs  
235 of 'typical' solutions present with multiple circular and elliptical vesicles (Fig. 2a-c). Some vesicles can  
236 become elongated and others encapsulated within larger vesicles (Fig. 2b and c). Vesicles are generally  
237 floating in solution unobstructed during analysis and display some flow caused by capillary action on  
238 the glass slide and erratic movement likely due to Brownian motion (SI video). TEM is performed under  
239 vacuum and as such the resulting micrographs contain collapsed or 'doughnut' shaped vesicles (Fig.  
240 2d-f). These would have been spherical in shape prior to being exposed to the vacuum pressure.

241 Table 1. Full details for each figure panel. SCA – single-chain amphiphile; FA – fatty acid; OH – alcohol; GOH – geraniol.

Figure	Microscopy	Scale bar	SCAs	pH	Formation temperature (°C)	Ionic species	Additional components	Morphologies	Size range
2 (a)	confocal	10 μm	C12 + C14 FAs, C10 OH	7.5	70	NA	Tris buffer	circular, elliptical, encapsulated	<10 μm
2 (b)	confocal	10 μm	C10 FA and OH	7.8	70	NA	NA	circular, elliptical, encapsulated, elongated, chains	<10 μm
2 (c)	confocal	10 μm	C10 FA, C10 OH	7.8	70	NA	NA	circular, elliptical, encapsulated, elongated	<10 μm
2 (d)	transmission electron	1 μm	C10 FA, C10 OH	12	70	HCO <sup>3-</sup>	NA	circular, elongated, chains	<1 μm
2 (e)	transmission electron	1 μm	C10, C11, C12, C13, C14, C15 FAs	7.5	70	NA	NA	collapsed/ "doughnut"	<1 μm
2 (f)	transmission electron	200 nm	C10, C11, C12, C13, C14, C15 FAs and OHs	8.8	70	NA	NA	collapsed/ "doughnut"	ca. 200 nm
3 (a)	confocal	10 μm	C10, C11, C12, C13, C14, C15 FAs and OHs	9.5	70	NA	NA	circular, laminated, curved-rod	ca. <1 to 50 μm

3 (b)	confocal	10 $\mu\text{m}$	C10, C11, C12, C13, C14, C15 FAs	9.3	70	NA	NA	chains, filaments, clusters	ca. 2 to >50 $\mu\text{m}$
3 (c)	confocal	10 $\mu\text{m}$	C10, C11, C12, C13, C14, C15 FAs	8.4	70	NA	NA	chains, filaments, clusters	ca. 2 to >50 $\mu\text{m}$
3 (d)	confocal	10 $\mu\text{m}$	C10, C11, C12, C13, C14, C15 FAs and OHs	8	70	NA	NA	clusters, appendages	<10 $\mu\text{m}$
3 (e)	confocal	10 $\mu\text{m}$	C10 FA and OH	7.3	70	NA	Tris buffer	circular, elliptical, aligned	<10 $\mu\text{m}$
3 (f)	confocal	10 $\mu\text{m}$	C10 FA and GA	13	70	$\text{HCO}_3^-$	NA	circular, elliptical, filaments, chains	<100 $\mu\text{m}$
4 (a)	transmission electron	1 $\mu\text{m}$	C10, C11, C12, C13, C14, C15 FAs	ca. 12	70	NaCl	NA	filaments/chains	>10 $\mu\text{m}$
4 (b)	transmission electron	200 nm	C10, C11, C12, C13, C14, C15 FAs and OHs	9.1	70	NA	cysteine	filaments, collapsed/ "doughnut"	<1 $\mu\text{m}$
4 (c)	transmission electron	1 $\mu\text{m}$	C10, C11, C12, C13, C14, C15 FAs and OHs	12	70	NaCl	NA	circular, symmetrical	<1 $\mu\text{m}$

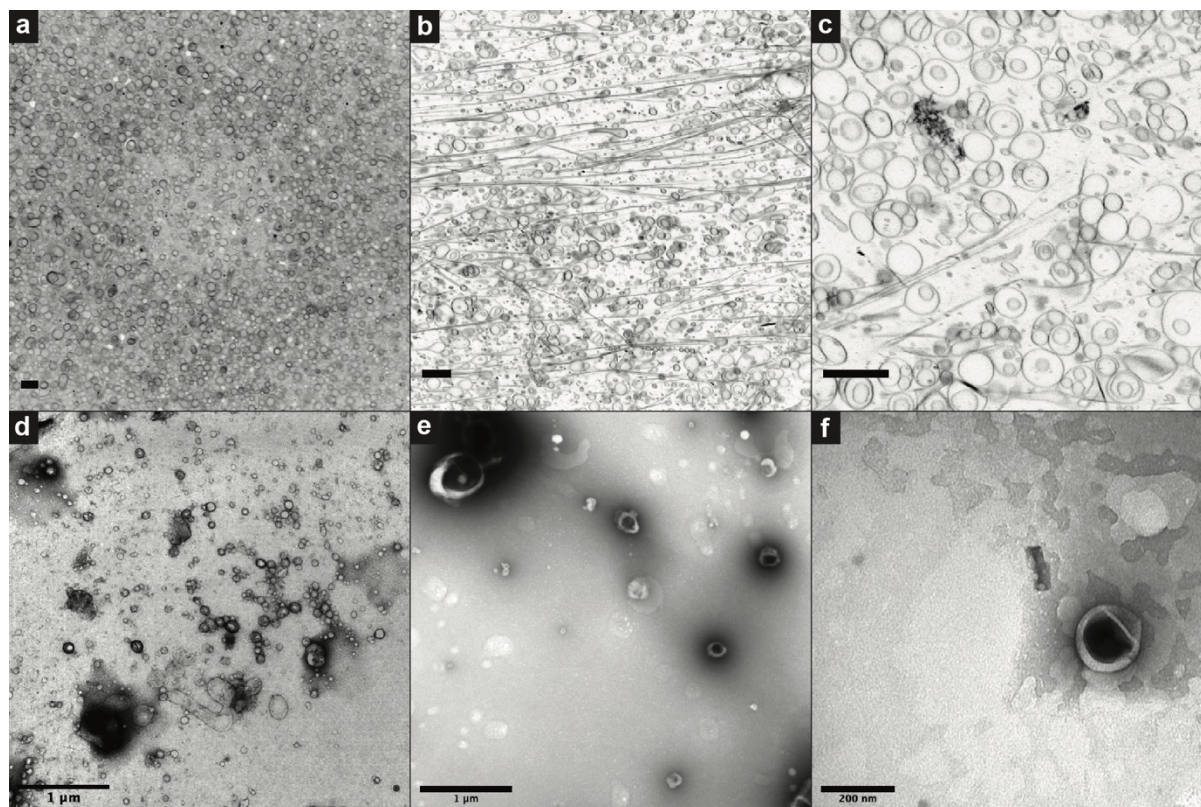
4 (d)	transmission electron	10 $\mu\text{m}$	C10 FA and GOH	12	70	$\text{FeCl}_3$	NA	filaments, clusters, dendritic	<50 $\mu\text{m}$
4 (e)	transmission electron	1 $\mu\text{m}$	C10 FA and GOH	12	70	$\text{HCO}_3^-$	NA	circular, collapsed/"doughnut", clusters	<1 $\mu\text{m}$
4 (f)	transmission electron	1 $\mu\text{m}$	C10, C11, C12, C13, C14, C15 FAs	11	70	Hydrothermal seawater <sup>51</sup>		circular, collapsed/"doughnut"	<100 nm
7 (a)	petrographic <sup>52</sup>	10 $\mu\text{m}$	NA	NA	NA	NA	suggested microfossils	circular, elliptical, clusters	<5 $\mu\text{m}$
7 (b)	petrographic <sup>53</sup>	10 $\mu\text{m}$	NA	NA	NA	NA	suggested microfossils	circular, elongated, clusters	<5 $\mu\text{m}$
7 (c)	petrographic <sup>54</sup>	10 $\mu\text{m}$	NA	NA	NA	NA	suggested microfossils	irregular circles	ca. 10 $\mu\text{m}$
7 (d)	scanning electron <sup>55</sup>	10 $\mu\text{m}$	NA	NA	NA	NA	biomorphs	circular, clusters, filaments	<5 $\mu\text{m}$ to >50 $\mu\text{m}$
7 (e)	confocal	10 $\mu\text{m}$	C10, C11, C12, C13, C14, C15 FAs and OHs	9.1	70	NA	NA	circular, elongated, clusters	<10 $\mu\text{m}$

7 (f)	confocal	10 $\mu\text{m}$	C10 FA and OH	7.4	70	$\text{FeCl}_3$	NA	circular, elliptical, elongated, clusters, encapsulated	<10 $\mu\text{m}$
7 (g)	confocal	10 $\mu\text{m}$	C10 FA and GOH	7	70	$\text{CaCl}_2$	NA	circular, irregular circles, filament, encapsulated	<10 $\mu\text{m}$
7 (h)	transmission electron	10 $\mu\text{m}$	C10, C11, C12, C13, C14, C15 FAs	ca. 12	70	NaCl	NA	filaments	>50 $\mu\text{m}$

---

242

243



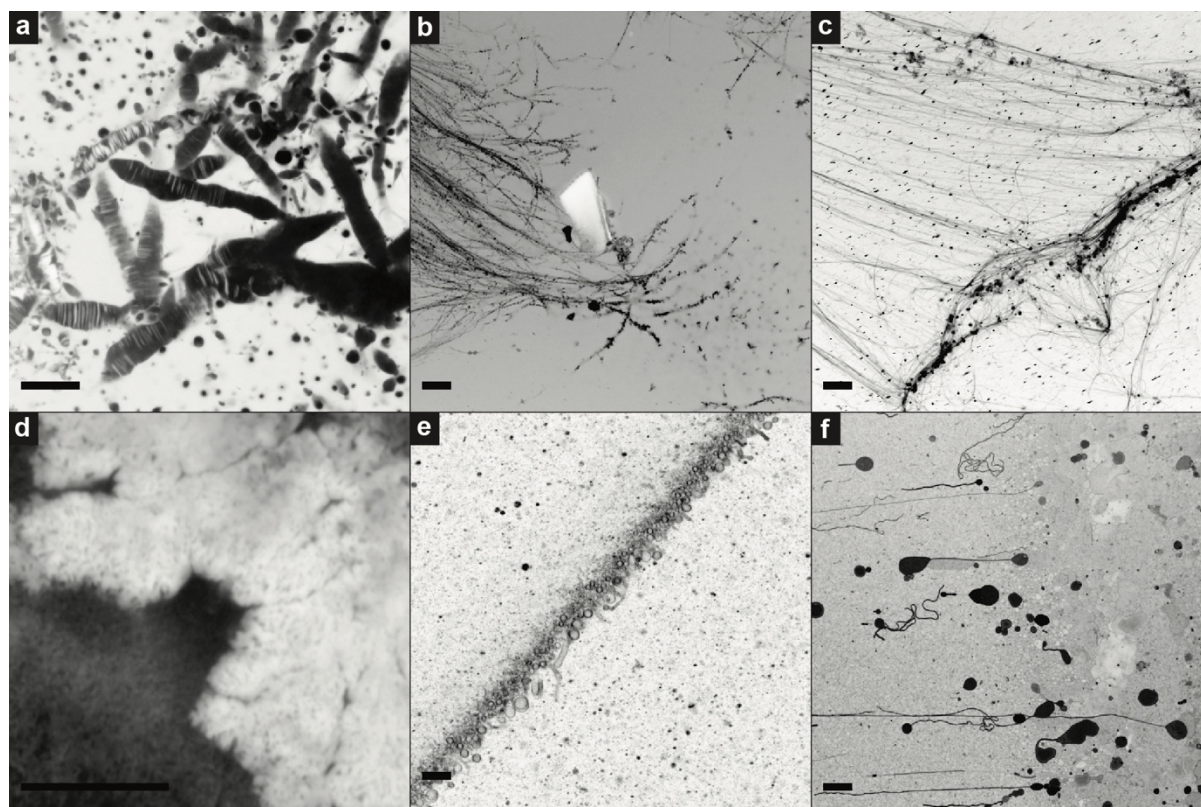
244

245 *Figure 2. Micrographs of images from ‘successful’ vesicle formation experiments. (a-c) Vesicles in*  
246 *solution imaged using confocal microscopy, (d-f) transmission electron micrographs of vesicles*  
247 *mounted on Cu grids. Scale bars are 10 μm (a-c), 1 μm (d and e) and 200 nm (f).*

248

249 As fluid flows on the glass slide during confocal analysis, some vesicles remain in place  
250 adhering to the glass and subsequently drying out. This can leave traces in a variety of shapes including  
251 laminated, curved-rods (Fig. 3a), large clusters with appendages (Fig. 3d), and filled circles or ellipses  
252 connected to filaments (Fig. 3f). Filaments are a common occurrence in solution (Fig. 3b and c)  
253 although their formation mechanism is unclear. Individual vesicles can also settle in formation while  
254 still in solution (e.g. linear formation in fig. 3e). This is likely due to a physical deformation in the glass  
255 slide which is linear in shape or the presence of a linear contaminant object to which the vesicles are  
256 attracted, potentially by surface charge interactions. Further work is necessary to elucidate the exact  
257 mechanisms behind these formations.

258



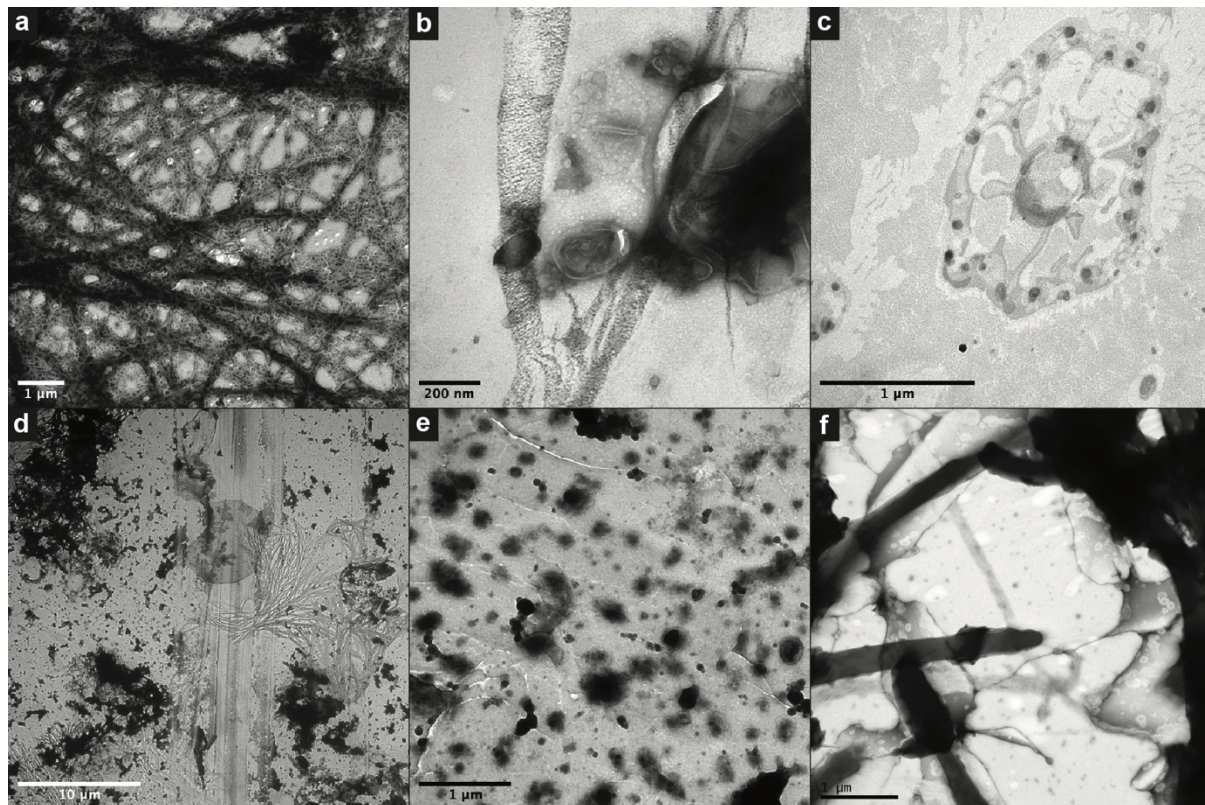
259

260 *Figure 3. Confocal micrographs of aggregates formed from solutions of organic molecules used in*  
261 *vesicle formation experiments. All scale bars are 10  $\mu$ m.*

262

263 The diversity of assemblage morphologies increases when analysed by TEM (Fig. 4). The  
264 vacuum clearly plays an important role here as in the drying during confocal analysis which also  
265 produced unique structures. Collapsed or 'doughnut' structures remain common but are often  
266 accompanied by filaments, chains, dendritic, and symmetrical patterns. The cause of these patterns is  
267 unclear although the presence of inorganic components in the solutions tends to increase the  
268 likelihood of complex morphologies. Some of the filamentous structures are comprised of individual  
269 vesicles and have been observed previously during confocal microscopy and subsequent TEM of the  
270 same solutions<sup>40</sup>. It was suggested that these filaments are the result of the organic vesicles being  
271 essentially salted-out of solution by the presence of inorganic salts such as NaCl.





272

273 *Figure 4. Transmission electron micrographs of aggregates formed from solutions of organic molecules*  
274 *used in vesicle formation experiments. Scale bars are 1 μm (a, c, e and f), 200 nm (b) and 10 μm (d).*

275

276 The population morphometry results for experimental vesicles were compared with a  
277 population of coccoidal cyanobacteria (Fig. 3a in Ref<sup>48</sup>,). For this latter image the exact same (updated)  
278 segmentation protocol was used (Fig. 5). The results are shown in Table 2, Fig. 6 and Fig. S4. Both  
279 circularity (C) and solidity (S) values for biomorph images (C = 0.83 – 0.84, S = 0.90 – 0.95) are similar  
280 to those of the cyanobacteria (C = 0.88, S = 0.96). The primary difference between biomorphs and  
281 microorganism in these analyses lies in the size measurement, where the cyanobacteria have a narrow  
282 size distribution (Fig. 6c, Fig. S4, radius mean/Std = 5.37) while the biomorphs have a radius mean/Std  
283 = 2.33 and radius mean/Std = 1.55 for dried and cryo experiments, respectively (Fig. 6b, c; Fig. S4).  
284 Overall, these data show that these organic biomorphs have a less uniform size distribution than  
285 typical single-strain populations of microbial cells, but that their shape may be indistinguishable. Given  
286 that a single parameter is not a reliable indicator, further experimentation is needed to expand our  
287 understanding of population morphometry in this area. Using a broader range of biomorphs, microbial  
288 populations, and microfossils will allow us to determine if there are statistically significant differences  
289 that will enable this approach to be used to determine biogenicity in the future.

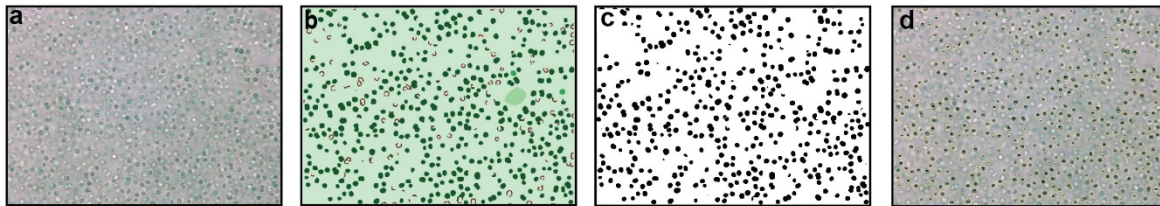
290

291

292 *Table 2. Particle characterisation parameters for Synechocystis sp. and biomorphs*

Sample	ID	Rad. M	Rad. Std	Rad. M/Std	Circ. M	Circ. Std	Circ. M/Std	Sol. M	Sol. Std	Sol. M/Std
Synechocystis	PCC	1.40	0.26	5.37	0.88	0.08	10.99	0.96	0.03	31.20
Biomorph-dried	DV	2.12	0.91	2.33	0.84	0.13	6.54	0.90	0.04	20.51
Biomorph-cryo	CV	14.40	9.28	1.55	0.83	0.09	9.57	0.95	0.03	30.89

293



294

295 *Figure 5. Image treatment for Synechocystis sp. (PCC6803), following the same protocol as for the*  
296 *experimental vesicles, shown in Fig. 1a) Original, cropped image, b) Weka trainable segmentation,*  
297 *separating artifacts from cells and background (see Fig. S3 for details), c) Tresholding and binarization,*  
298 *d) Particle counting, size and shape description. For more details on segmentation see Figure S3.*

299

300

301

302

303

304

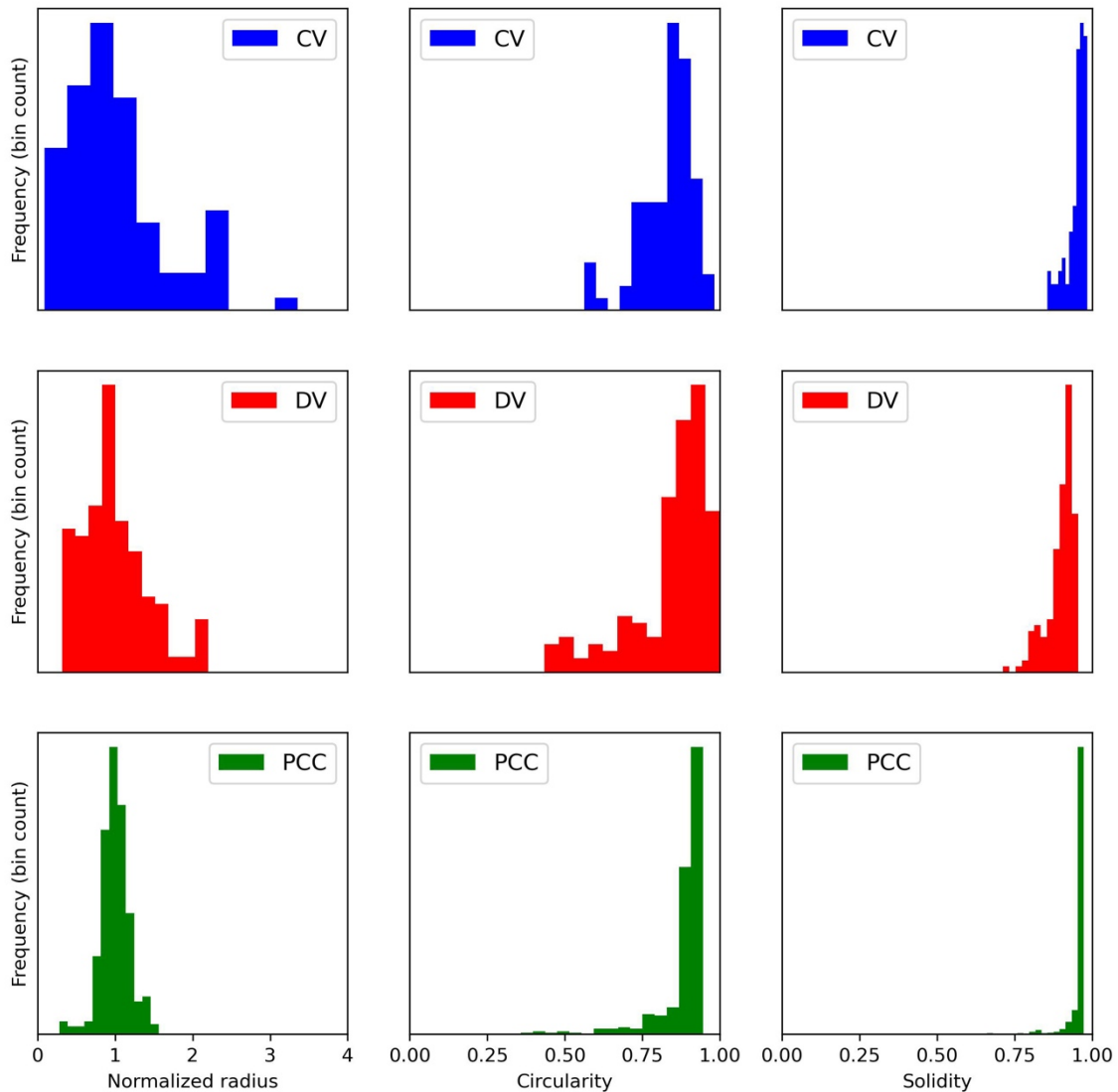
305

306

307

308

309



310

311 Figure 6. Distributions of normalized size, circularity and solidity of cryogenic vesicles (Fig. S2), dried  
312 vesicles (Fig. S1) and microbial cells (*Synechocystis sp.*, PCC6803, Fig. S3).

313

### 314 Discussion

315 Our results show that abiotic organic molecules, likely present on the early Earth, including fatty acids,  
316 1-alkanols, and isoprenoids are capable of forming a diverse range of complex morphologies. Confocal  
317 microscopy and TEM analyses provide insights into the possible forms observed using different  
318 analytical techniques. The microstructures are formed across a range of environmental conditions  
319 with varying pH, temperature, and ionic strength – each of which appear to affect structural  
320 morphology. The vast possible combinations of abiotic organic molecules, inorganic materials, and  
321 chemical conditions on the early Earth suggest that the formation of these kinds of biomorphs would  
322 have been inevitable. Yet our understanding of their formation mechanisms and diagnostic  
323 characteristics remains in its infancy, primarily due to a paucity of research in this area.

324

325 *Comparison with microfossils*

326 From the relatively small selection of abiotic mixtures presented here, a substantially diverse range of  
327 morphologies was observed some of which are reminiscent of suggested microfossils from Earth's  
328 early rock record (Fig. 7). Vesicle experiments were not directed in any way towards the replication of  
329 these or any microfossil morphologies. Yet, many microfossil morphologies reported in the Archean  
330 and Paleoproterozoic rock record appear to have comparable shapes and sizes. Clusters of  
331 carbonaceous spheroids and filaments, interpreted as ancient cell colonies, have been reported in e.g.  
332 3.4-3.2 Ga cherts of the Barberton Greenstone Belt (BGB), South Africa<sup>52,56-58</sup>, 3.5-3.0 Ga cherts of the  
333 Pilbara Granitoid-Greenstone Belt, Western Australia<sup>53,54,59-64</sup>, and the 1.9 Ga Gunflint Formation,  
334 Canada<sup>53,65,66</sup>. Some examples of morphological comparison between microfossils and  
335 experimentally-produced vesicles are shown in Figure 7.

336 For instance, spheroidal or spherule-like microfossils in the ca. 3.3-3.4 Ga Kromberg Formation  
337 within the BGB (Fig. 7a)<sup>52</sup>, are similar in shape to many abiotic vesicle micrographs including the  
338 example presented in Figure 5e which were formed from a mix of twelve fatty acids and 1-alkanols  
339 (C10 to C15) at alkaline pH (pH 9.1). Westall et al. (2001)<sup>52</sup> present several examples of spherules  
340 'joined in pairs', a feature which is also observed in vesicle solutions. They argue that their observed  
341 structures fulfil several biological criteria including size, morphology, cell division, colonial distribution,  
342 and cell wall texture. While we agree with this assessment, the vesicle experiments here also arguably  
343 meet these criteria. In another example, clusters of spheroidal microfossils, identified in the ca. 3.4  
344 Ga Strelley Pool Formation, Western Australia, and interpreted as remnants of sulphur-metabolising  
345 cells<sup>34</sup> (Fig. 7c), are similar in shape to the ca. 10 µm diameter circular vesicles formed in the laboratory  
346 from decanoic and geranic acid in the presence of CaCl<sub>2</sub> (Fig. 7g).

347 These morphological similarities extend to filamentous shapes and even to mixtures of  
348 spheroids and filaments. For example, Wacey et al. (2012)<sup>53</sup> reported a selection of spheroidal and  
349 filamentous microfossils (suggested Huroniospora and Siphonophycus/Gunflintia respectively) from  
350 within a stromatolitic chert of the ca. 1.9 Ga Gunflint Formation, Canada (Fig. 7b). We also observed  
351 these co-occurring morphologies in solutions of decanoic acid and 1-decanol containing FeCl<sub>3</sub> at pH  
352 7.4 (Fig. 7g), although combined circular and filamentous vesicle morphologies are not restricted to  
353 Fe-containing solutions. Considering the younger age of these microfossils a biogenic origin is likely  
354 but without more advanced data on the formation and preservation of abiotic microstructures it  
355 remains uncertain.

356 It should be noted that, although the vast majority of Archean and Paleoproterozoic  
357 microfossil morphologies are spheroidal or filamentous, other morphologies exist such as spindle-like

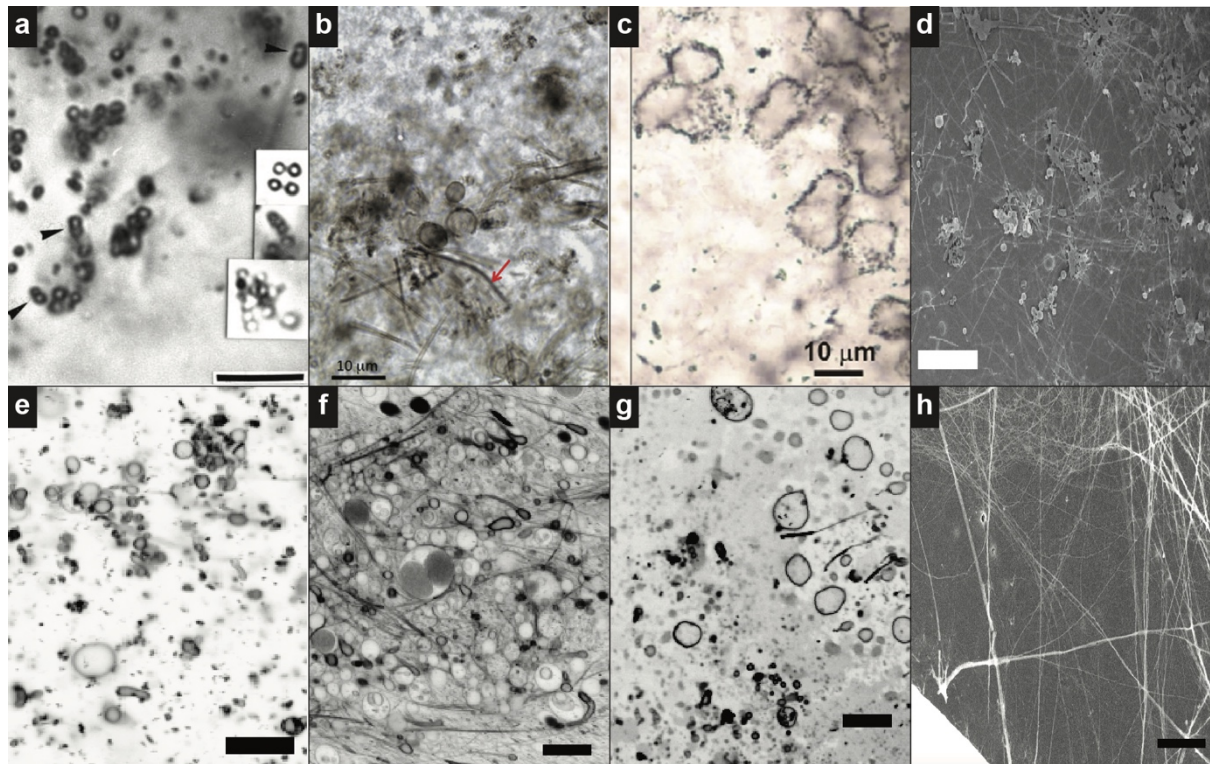
358 and lenticular shapes<sup>61,67,68</sup> and hollow tubular organic structures<sup>69</sup>, that do not appear to be  
359 mimicked in our current experiments. It may be possible that these morphologies result specifically  
360 from the larger molecules which make up prokaryotic cell walls (i.e., polysaccharides and proteins).  
361 Indeed, much of the biogenicity criteria employed for microfossil interpretation relates to interpreting  
362 cell wall morphology specifically. Further work is needed to elucidate this possibility. That lipid vesicles  
363 are chemically analogous to cell membranes rather than cell walls should not however affect their  
364 relevance to microfossil interpretation. In chemical terms, following billions of years of diagenesis,  
365 organic molecules will largely have been converted to graphite regardless of the complexity of their  
366 original form. Some of the biomorph morphologies presented here result from individual vesicles  
367 forming individual spherical shapes (e.g., Fig. 2a). Others, such as the filamentous structures, are  
368 formed from aggregates of individual vesicles (e.g., Fig. 4a). In addition, it has been shown previously  
369 that vesicles can bind to and coat mineral particles, likely due to surface charge interactions, creating  
370 an organic cast of the mineral shape<sup>41</sup>. Self-assembly of abiotic SCAs may yet yield these additional  
371 morphologies, particularly in conjunction with relevant inorganic species. Moreover, detailed physical  
372 and chemical analyses of organic biomorphs will allow us to better understand their relevance to  
373 microfossil interpretation.

374 It is important to realize that up to this point only the morphological aspects of these  
375 abiogenic vesicles have been studied and compared to ancient microfossils. In recent years, however,  
376 it has become possible to image and characterize individual microfossils using in-situ analytical  
377 techniques such as Raman spectroscopy, confocal laser scanning microscopy (CLSM), Secondary ion  
378 mass spectrometry (SIMS, NanoSIMS), transmission electron microscopy and energy-dispersive X-ray  
379 spectroscopy (TEM-EDXS), and synchrotron-based scanning transmission X-ray spectroscopy (STXM).  
380 Combinations of these techniques make it possible to directly link chemical and isotopic  
381 characteristics to the morphology of microfossils. A recent overview of these techniques for the study  
382 of microfossils is given in Lepot (2020)<sup>70</sup>. It is thus important to note that some of the examples of  
383 microfossils given above have been studied using additional chemical and isotopic analyses. For the  
384 spheroidal microfossils identified by Wacey et al. (2011)<sup>54</sup> in the ca. 3.4 Ga Strelley Pool Formation,  
385 Western Australia (Fig. 7c), specific SIMS-based  $\delta^{13}\text{C}$  and  $\delta^{34}\text{S}$  analyses provided evidence for sulphur-  
386 based metabolism. For the filamentous and spheroidal microfossils of the 1.9 Ga Gunflint Formation  
387 Wacey et al. (2012)<sup>53</sup> (Fig. 7b) performed more advanced morphological and elemental analyses  
388 utilising focused ion beam (FIB) milling in combination with SEM and TEM to provide micrographs of  
389 both nanoscale resolution and in three dimensions. In general, a range of chemical- and isotopic  
390 biogenicity criteria have thus been created that can be directly linked to the classical morphology-  
391 based biogenicity criteria. To date, this analytical approach has not been applied to abiotic vesicle



392 experiments although it is clearly necessary to provide control data for these kinds of microfossil  
393 investigations.

394



395

396 *Figure 7. Comparison between purported microfossils and vesicle aggregates. Panels a-c are published*  
397 *micrographs of controversial microfossils (a - Westall et al. (2001), b - Wacey et al. (2012), c - Wacey*  
398 *et al. (2011)), d is a published micrograph of a biomorph from Cosmidis and Templeton (2016) formed*  
399 *from sulfur and yeast extract, and panels e-h are micrographs of vesicles that were produced during*  
400 *this study. All scale bars are 10  $\mu\text{m}$ .*

401

#### 402 *Comparison with other organic biomorphs*

403 Previous work from Cosmidis and Templeton<sup>55</sup> investigating the potential formation of carbon/sulfur-  
404 based biomorphs produced a variety of spheroidal and filamentous structures (Fig. 7d) which  
405 resemble the morphologies of filamentous vesicle solutions (Fig. 7h). This highlights the potential for  
406 abiotic organic compounds from multiple sources to form microstructures that mimic microfossils.  
407 The authors in this case call for ‘new caution’ in interpreting putative microfossils in the rock record<sup>55</sup>.  
408 In a recent study Nims et al.<sup>71</sup> produced biomorphs containing sulphur and organic carbon which were  
409 morphologically reminiscent of the filamentous sulphur-oxidizing bacteria *Thiothrix* containing  
410 intracellular sulphur globules. Future isotopic analyses performed on these biomorphs could provide  
411 some initial control data for sulphur and carbon containing microfossil interpretation. More  
412 experimental work of this kind is imperative for our interpretation of microstructures in the rock

413 record. In another recent study Criouet et al. (2021)<sup>72</sup> showed experimentally that under diagenetic  
414 conditions RNA molecules mixed with quartz and water will create spheroidal organic microstructures  
415 that mimic microorganisms such as Staphylococcus or Thermococcales. With these types of studies,  
416 we are beginning to see only the tip of the iceberg of the potential for organic biomorphs to obscure  
417 the rock record.

418

#### 419 *Relevance for biogenicity tests*

420 Recently it has been suggested that the development of a strong set of criteria for determining the  
421 biogenicity of microfossils is crucial to our understanding of the Earth's early biosphere<sup>73</sup>. Clearly the  
422 design of such criteria necessitates knowledge of the potential for abiotic structures to obscure our  
423 interpretations. These microstructures may provide answers to questions that currently overshadow  
424 uninterpreted signatures which have been observed in rock samples. It is essential that we understand  
425 the formation and preservation of these structures particularly following diagenetic processes  
426 representative of those experienced by relevant geological materials. Without the requisite control  
427 data, we may continue to struggle through ambiguity. Understanding the composition of these non-  
428 living structures would not only improve our interpretation of potential microfossils, but it could also  
429 shed light on the environment in which abiotic structures were formed, further adding to our  
430 knowledge of Earth's history. Furthermore, these biomorphs may be particularly beneficial for the  
431 analysis of potential biosignatures on other planets where life may have started but perhaps did not  
432 evolve in complexity. This is critical for the development of strategies for life-detection and  
433 instruments for future space missions<sup>73-75</sup>. With sample return from Mars likely to be realised in the  
434 not too distant future, it is essential that we are prepared to provide the best possible interpretation  
435 of any proposed biosignatures that we identify during investigations here on Earth.

436

#### 437 **Conclusions**

438 The current study presents a direct link between the origin of life and microfossil interpretation. We  
439 have shown that lipid vesicles, representative of the first stages of cell membrane development at the  
440 emergence of life, are capable of satisfying morphology criteria applied to traces of life from the early  
441 Earth, and the development of advanced statistical approaches is required to pinpoint potential  
442 differences which may enable us to distinguish between biogenic and abiogenic structures. It has been  
443 suggested that the preserved remnants of prebiotic chemistry could potentially satisfy many of the  
444 widely accepted biogenicity criteria currently applied to possible microfossils<sup>75</sup>. The work presented  
445 here represents a miniscule fragment of all possible prebiotic biomorphs which could be observed in  
446 geological samples from the early Earth and potentially elsewhere in the Solar System. These



447 biomorphs could also inform on potential fossilised signatures of life's emergence which could be  
448 observed in either terrestrial or extra-terrestrial samples – protobiosignatures. A significant effort is  
449 required to determine the full range of possible prebiotic biomorphs which could affect our  
450 interpretation of the earliest rock record including advanced physical, chemical, and statistical  
451 analytical approaches.

452

#### 453 **Author contributions**

454 Conceptualisation, S.F.J. and M.A.vZ.; Methodology, S.F.J, M.A.vZ., and J.R.; Experiments and analysis,  
455 S.F.J., M.A.vZ., and J.R.; Writing—original draft, S.F.J.; Writing—review & editing, S.F.J., M.A.vZ., J.R.,  
456 Z.M., and N.L.; Project administration, S.F.J.; Funding acquisition, S.F.J, M.A.vZ., Z.M., and N.L.. All  
457 authors have read and agreed to the published version of the manuscript.

458

#### 459 **Acknowledgements**

460 We thank Mark Turmaine and Andrew M. Hartley for assistance with NS-TEM and Cryo-EM  
461 experiments, respectively. S.F.J. acknowledges support from “la Caixa” Foundation (ID  
462 100010434) and from the European Union’s Horizon 2020 research and innovation programme under  
463 the Marie Skłodowska Curie grant agreement No 847648. The fellowship code is  
464 “LCF/BQ/PI21/11830015”. Centro de Química Estrutural acknowledges the financial support of  
465 Fundação para a Ciência e Tecnologia (FCT) through projects UIDB/00100/2020 and  
466 UIDP/00100/2020. Institute of Molecular Sciences acknowledges the financial support of FCT through  
467 project LA/P/0056/2020. Z.M. acknowledges funding from Fundação para a Ciência a Tecnologia (FCT)  
468 grant number 2022.05284.PTDC.

469

#### 470 **References**

- 471 1. Damer, B. & Deamer, D. The Hot Spring Hypothesis for an Origin of Life. *Astrobiology* **20**, 429–  
472 452 (2019).
- 473 2. Russell, M. J. & Hall, A. J. The emergence of life from iron monosulphide bubbles at a  
474 submarine hydrothermal redox and pH front. *J Geol Soc London* **154**, 377–402 (1997).
- 475 3. Russell, M. J. & Martin, W. The rocky roots of the acetyl-CoA pathway. *Trends Biochem Sci* **29**,  
476 358–363 (2004).
- 477 4. Preiner, M. *et al.* A hydrogen-dependent geochemical analogue of primordial carbon and  
478 energy metabolism. *Nat Ecol Evol* (2020) doi:10.1038/s41559-020-1125-6.
- 479 5. Muchowska, K. B., Varma, S. J. & Moran, J. Synthesis and breakdown of universal metabolic  
480 precursors promoted by iron. *Nature* **569**, 104–107 (2019).

- 481 6. Harrison, S. A. *et al.* Life as a guide to its own origins. *Annu Rev Ecol Evol Syst* (2023).
- 482 7. Nunes Palmeira, R., Colnaghi, M., Harrison, S. A., Pomiankowski, A. & Lane, N. The limits of  
483 metabolic heredity in protocells. *Proceedings of the Royal Society B: Biological Sciences* **289**,  
484 (2022).
- 485 8. West, T., Sojo, V., Pomiankowski, A. & Lane, N. The origin of heredity in protocells.  
486 *Philosophical Transactions of the Royal Society B: Biological Sciences* **372**, (2017).
- 487 9. Lombard, J., López-García, P. & Moreira, D. The early evolution of lipid membranes and the  
488 three domains of life. *Nat Rev Microbiol* **10**, 507–515 (2012).
- 489 10. Hargreaves, W. R. & Deamer, D. W. Liposomes from ionic, single-chain amphiphiles.  
490 *Biochemistry* **17**, 3759–3768 (1978).
- 491 11. Oro, J. Chemical synthesis of lipids and the origin of life. *J Biol Phys* **20**, 135–147 (1995).
- 492 12. McCollom, T. M. Miller-Urey and beyond: What have we learned about prebiotic organic  
493 synthesis reactions in the past 60 years? *Annu Rev Earth Planet Sci* **41**, 207–229 (2013).
- 494 13. McCollom, T. M., Ritter, G. & Simoneit, B. R. T. Lipid synthesis under hydrothermal conditions  
495 by Fischer-Tropsch reactions. *Origins of life and evolution of the biosphere* **29**, 153–166  
496 (1999).
- 497 14. Miller, S. L. A Production of Amino Acids Under Possible Primitive Earth Conditions. *Science*  
498 (1979) **117**, 528 LP – 529 (1953).
- 499 15. Cairns-Smith, A. G., Ingram, P. & Walker, G. L. Formose production by minerals: Possible  
500 relevance to the origin of life. *J Theor Biol* **35**, 601–604 (1972).
- 501 16. Stairs, S. *et al.* Divergent prebiotic synthesis of pyrimidine and 8-oxo-purine ribonucleotides.  
502 *Nat Commun* **8**, 15270 (2017).
- 503 17. Keller, M. A., Kampjut, D., Harrison, S. A. & Ralser, M. Sulfate radicals enable a non-enzymatic  
504 Krebs cycle precursor. *Nat Ecol Evol* **1**, 83 (2017).
- 505 18. Keller, M. A., Turchyn, A. V & Ralser, M. Non-enzymatic glycolysis and pentose phosphate  
506 pathway-like reactions in a plausible Archean ocean. *Mol Syst Biol* **10**, 725 (2014).
- 507 19. Messner, C. B., Driscoll, P. C., Piedrafita, G., De Volder, M. F. L. & Ralser, M. Nonenzymatic  
508 gluconeogenesis-like formation of fructose 1,6-bisphosphate in ice. *Proc Natl Acad Sci U S A*  
509 **114**, 7403–7407 (2017).
- 510 20. Muchowska, K. B., Varma, S. J. & Moran, J. Nonenzymatic Metabolic Reactions and Life's  
511 Origins. *Chem Rev* **120**, 7708–7744 (2020).
- 512 21. Camprubi, E. *et al.* Do Soluble Phosphates Direct the Formose Reaction towards Pentose  
513 Sugars? *Astrobiology* **22**, 981–991 (2022).

- 514 22. Pinna, S. *et al.* A prebiotic basis for ATP as the universal energy currency. *PLoS Biol* **20**,  
515 e3001437 (2022).
- 516 23. Harrison, S. A., Webb, W. L., Ramm, H. & Lane, N. Prebiotic Synthesis of Aspartate Using  
517 Life's Metabolism as a Guide. *Life* **13**, (2023).
- 518 24. Martins, Z. Organic Molecules in Meteorites and Their Astrobiological Significance. in  
519 *Handbook of Astrobiology* (ed. Kolb, V. M.) 177–194 (CRC Press, 2019).
- 520 25. Martins, Z. Organic Molecules in Meteorites and Their Astrobiological Significance. in  
521 *Handbook of Astrobiology* (ed. Kolb, V. M.) 177–194 (CRC Press, 2019).
- 522 26. Lai, J. C.-Y., Pearce, B. K. D., Pudritz, R. E. & Lee, D. Meteoritic abundances of fatty acids and  
523 potential reaction pathways in planetesimals. *Icarus* **319**, 685–700 (2019).
- 524 27. Huang, Y. *et al.* Molecular and compound-specific isotopic characterization of monocarboxylic  
525 acids in carbonaceous meteorites. *Geochim Cosmochim Acta* **69**, 1073–1084 (2005).
- 526 28. Aponte, J. C. *et al.* Effects of secondary alteration on the composition of free and IOM-  
527 derived monocarboxylic acids in carbonaceous chondrites. *Geochim Cosmochim Acta* **75**,  
528 2309–2323 (2011).
- 529 29. Cooper, G. W. & Cronin, J. R. Linear and cyclic aliphatic carboxamides of the Murchison  
530 meteorite: Hydrolyzable derivatives of amino acids and other carboxylic acids. *Geochim*  
531 *Cosmochim Acta* **59**, 1003–1015 (1995).
- 532 30. Martins, Z. *et al.* Free dicarboxylic and aromatic acids in the carbonaceous chondrites  
533 Murchison and Orgueil. *Meteorit Planet Sci* **41**, 1073–1080 (2006).
- 534 31. Deamer, D. W. Boundary structures are formed by organic components of the Murchison  
535 carbonaceous chondrite. *Nature* **317**, 792–794 (1985).
- 536 32. Deamer, D. W. & Pashley, R. M. Amphiphilic components of the murchison carbonaceous  
537 chondrite: Surface properties and membrane formation. *Origins of life and evolution of the*  
538 *biosphere* **19**, 21–38 (1989).
- 539 33. Hopkins, M. D. & Mojzsis, S. J. A protracted timeline for lunar bombardment from mineral  
540 chemistry, Ti thermometry and U–Pb geochronology of Apollo 14 melt breccia zircons.  
541 *Contributions to Mineralogy and Petrology* **169**, 30 (2015).
- 542 34. Pearce, B. K. D., Tupper, A. S., Pudritz, R. E. & Higgs, P. G. Constraining the Time Interval for  
543 the Origin of Life on Earth. *Astrobiology* **18**, 343–364 (2018).
- 544 35. Monnard, P.-A., Apel, C. L., Kanavarioti, A. & Deamer, D. W. Influence of ionic inorganic  
545 solutes on self-assembly and polymerization processes related to early forms of life:  
546 implications for a prebiotic aqueous medium. *Astrobiology* **2**, 139–152 (2002).

- 547 36. Monnard, P. A. & Deamer, D. W. Membrane self-assembly processes: Steps toward the first  
548 cellular life. *The Minimal Cell: The Biophysics of Cell Compartment and the Origin of Cell*  
549 *Functionality* **207**, 123–151 (2002).
- 550 37. Szostak, J. W., Bartel, D. P. & Luisi, P. L. Synthesizing life. *Nature* **409**, 387–390 (2001).
- 551 38. Deamer, D. The Role of Lipid Membranes in Life's Origin. *Life* **7**, 5 (2017).
- 552 39. Maurer, S. E. *et al.* Vesicle self-assembly of monoalkyl amphiphiles under the effects of high  
553 ionic strength, extreme pH, and high temperature environments. *Langmuir* **34**, 15560–15568  
554 (2018).
- 555 40. Jordan, S. F. *et al.* Promotion of protocell self-assembly from mixed amphiphiles at the origin  
556 of life. *Nat Ecol Evol* **3**, 1705–1714 (2019).
- 557 41. Jordan, S. F., Nee, E. & Lane, N. Isoprenoids enhance the stability of fatty acid membranes at  
558 the emergence of life potentially leading to an early lipid divide. *Interface Focus* **9**, 20190067  
559 (2019).
- 560 42. García-Ruiz, J. M. *et al.* Self-Assembled Silica-Carbonate Structures and Detection of Ancient  
561 Microfossils. *Science (1979)* **302**, 1194 LP – 1197 (2003).
- 562 43. Rouillard, J., García-Ruiz, J. M., Gong, J. & van Zuilen, M. A. A morphogram for silica-witherite  
563 biomorphs and its application to microfossil identification in the early earth rock record.  
564 *Geobiology* **16**, 279–296 (2018).
- 565 44. García-Ruiz, J. M., Melero-García, E. & Hyde, S. T. Morphogenesis of Self-Assembled  
566 Nanocrystalline Materials of Barium Carbonate and Silica. *Science (1979)* **323**, 362 LP – 365  
567 (2009).
- 568 45. Kotopoulou, E., Lopez-Haro, M., Calvino Gamez, J. J. & García-Ruiz, J. M. Nanoscale Anatomy  
569 of Iron-Silica Self-Organized Membranes: Implications for Prebiotic Chemistry. *Angewandte*  
570 *Chemie International Edition* **60**, 1396–1402 (2021).
- 571 46. Monnard, P. A. & Deamer, D. W. Preparation of vesicles from nonphospholipid amphiphiles.  
572 *Methods Enzymol* **372**, 133–151 (2003).
- 573 47. Lane, N. & Martin, W. F. The origin of membrane bioenergetics. *Cell* **151**, 1406–1416 (2012).
- 574 48. Rouillard, J., van Zuilen, M., Pisapia, C. & Garcia-Ruiz, J.-M. An Alternative Approach for  
575 Assessing Biogenicity. *Astrobiology* **21**, 151–164 (2021).
- 576 49. Rouillard, J. *et al.* Identifying microbial life in rocks: Insights from population morphometry.  
577 *Geobiology* **18**, 282–305 (2020).
- 578 50. Arganda-Carreras, I. *et al.* Trainable Weka Segmentation: a machine learning tool for  
579 microscopy pixel classification. *Bioinformatics* **33**, 2424–2426 (2017).

- 580 51. Zaia, D. A. M. Adsorption of amino acids and nucleic acid bases onto minerals: A few  
581 suggestions for prebiotic chemistry experiments. *Int J Astrobiol* **11**, 229–234 (2012).
- 582 52. Westall, F. *et al.* Early Archean fossil bacteria and biofilms in hydrothermally-influenced  
583 sediments from the Barberton greenstone belt, South Africa. *Precambrian Res* **106**, 93–116  
584 (2001).
- 585 53. Wacey, D. *et al.* Taphonomy of very ancient microfossils from the ~3400Ma Strelley Pool  
586 Formation and ~1900Ma Gunflint Formation: New insights using a focused ion beam.  
587 *Precambrian Res* **220–221**, 234–250 (2012).
- 588 54. Wacey, D., Kilburn, M. R., Saunders, M., Cliff, J. & Brasier, M. D. Microfossils of sulphur-  
589 metabolizing cells in 3.4-billion-year-old rocks of Western Australia. *Nat Geosci* **4**, 698–702  
590 (2011).
- 591 55. Cosmidis, J. & Templeton, A. S. Self-assembly of biomorphic carbon/sulfur microstructures in  
592 sulfidic environments. *Nat Commun* **7**, 12812 (2016).
- 593 56. Cavalazzi, B. *et al.* Cellular remains in a ~3.42-billion-year-old seafloor hydrothermal  
594 environment. *Sci Adv* **7**, eabf3963 (2022).
- 595 57. Javaux, E. J., Marshall, C. P. & Bekker, A. Organic-walled microfossils in 3.2-billion-year-old  
596 shallow-marine siliciclastic deposits. *Nature* **463**, 934–938 (2010).
- 597 58. Kremer, B. & Kaźmierczak, J. Cellularly preserved microbial fossils from ~3.4Ga deposits of  
598 South Africa: A testimony of early appearance of oxygenic life? *Precambrian Res* **295**, 117–  
599 129 (2017).
- 600 59. Coutant, M. *et al.* Distinguishing cellular from abiotic spheroidal microstructures in the ca.  
601 3.4 Ga Strelley Pool Formation. *Geobiology* **20**, 599–622 (2022).
- 602 60. Schopf, J. W. Microfossils of the Early Archean Apex Chert: New Evidence of the Antiquity of  
603 Life. *Science (1979)* **260**, 640–646 (1993).
- 604 61. Sugitani, K., Mimura, K., Nagaoka, T., Lepot, K. & Takeuchi, M. Microfossil assemblage from  
605 the 3400Ma Strelley Pool Formation in the Pilbara Craton, Western Australia: Results form a  
606 new locality. *Precambrian Res* **226**, 59–74 (2013).
- 607 62. Sugitani, K., Grey, K., Nagaoka, T., Mimura, K. & Walter, M. R. Taxonomy and biogenicity of  
608 Archaean spheroidal microfossils (ca. 3.0Ga) from the Mount Goldsworthy–Mount Grant area  
609 in the northeastern Pilbara Craton, Western Australia. *Precambrian Res* **173**, 50–59 (2009).
- 610 63. Sugitani, K. *et al.* Diverse microstructures from Archaean chert from the Mount Goldsworthy–  
611 Mount Grant area, Pilbara Craton, Western Australia: Microfossils, dubiofossils, or  
612 pseudofossils? *Precambrian Res* **158**, 228–262 (2007).

- 613 64. Wacey, D., Saunders, M., Kong, C., Brasier, A. & Brasier, M. 3.46Ga Apex chert ‘microfossils’  
614 reinterpreted as mineral artefacts produced during phyllosilicate exfoliation. *Gondwana*  
615 *Research* **36**, 296–313 (2016).
- 616 65. Alleon, J. *et al.* Early entombment within silica minimizes the molecular degradation of  
617 microorganisms during advanced diagenesis. *Chem Geol* **437**, 98–108 (2016).
- 618 66. Lepot, K. *et al.* Iron minerals within specific microfossil morphospecies of the 1.88 Ga Gunflint  
619 Formation. *Nat Commun* **8**, 14890 (2017).
- 620 67. Oehler, D. Z., Walsh, M. M., Sugitani, K., Liu, M.-C. & House, C. H. Large and robust lenticular  
621 microorganisms on the young Earth. *Precambrian Res* **296**, 112–119 (2017).
- 622 68. Sugitani, K. *et al.* Biogenicity of Morphologically Diverse Carbonaceous Microstructures from  
623 the ca. 3400 Ma Strelley Pool Formation, in the Pilbara Craton, Western Australia.  
624 *Astrobiology* **10**, 899–920 (2010).
- 625 69. Kaźmierczak, J., Kremer, B., Altermann, W. & Franchi, I. Tubular microfossils from ~2.8 to  
626 2.7Ga-old lacustrine deposits of South Africa: A sign for early origin of eukaryotes?  
627 *Precambrian Res* **286**, 180–194 (2016).
- 628 70. Lepot, K. Signatures of early microbial life from the Archean (4 to 2.5 Ga) eon. *Earth Sci Rev*  
629 **209**, 103296 (2020).
- 630 71. Nims, C., Lafond, J., Alleon, J., Templeton, A. S. & Cosmidis, J. Organic biomorphs may be  
631 better preserved than microorganisms in early Earth sediments. *Geology* **49**, 629–634 (2021).
- 632 72. Criouet, I., Viennet, J.-C., Jacquemot, P., Jaber, M. & Bernard, S. Abiotic formation of organic  
633 biomorphs under diagenetic conditions. *Geochem Perspect Lett* **16**, 40–46 (2021).
- 634 73. Javaux, E. J. Challenges in evidencing the earliest traces of life. *Nature* **572**, 451–460 (2019).
- 635 74. McMahon, S. & Cosmidis, J. False biosignatures on Mars: anticipating ambiguity. *J Geol Soc*  
636 *London* **179**, (2022).
- 637 75. McMahon, S. & Jordan, S. F. A fundamental limit to the search for the oldest fossils. *Nat Ecol*  
638 *Evol* (2022) doi:10.1038/s41559-022-01777-0.
- 639